International Forum on Aeroelasticity and Structural Dynamics
IFASD 2024
17-21 June 2024, The Hague, The Netherlands

PASSIVE AND ACTIVE LOAD ALLEVIATION TECHNOLOGIES FOR UHARW WINGS

Francesco Toffol[1]

[1] Department of Aerospace Science and Technology

Politecnico di Milano,

Via la Masa 34, 20156, Milano.

Italy

Keywords: Gust Load Alleviation, Folding Wing Tip, Active Control

Abstract: In the framework of the Ultra High Aspect Ratio Wing Advanced Research and Designs (U-HARWARD) CS2JU founded project, different gust load alleviation (GLA) technologies were developed and studied. GLA is a key enabler for the development of new generation UHARW, indeed the GLA allows to limit the gust loads and as a direct consequence it can reduce the structural weight of the wing itself and considering the snowball effect of the entire aircraft. This overall weight reduction improves the global aircraft efficiency allowing an increase in the aspect ratio.

GLA technologies can be divided into two main categories: the passive ones where no action is needed to reduce the load and the active ones where a control system modifies the aerodynamic loads automatically. In this case, the passive GLA is performed with a Folding Wing Tip (FWT) developed by the University of Bristol and the GLA is performed with a Static Output Feedback controller developed by Politecnico di Milano. Both cases are compared with the baseline aircraft.

A flutter assessment is performed to prove that the FWT do not introduces aeroelastic instabilities and the aircraft is flutter free across the entire flight envelope when the FWT is free to float.

A comprehensive comparison of the load envelopes obtained is provided, considering almost 2000 load cases for different flight points and mass configurations for the baseline aircraft and the GLA solutions. The gust cases are compliant with CS25 regulations and account for positive and negative cases, providing the bending-torsion envelopes in different spanwise placed monitoring stations.

Thanks to NeOPT it was possible to realize a hybrid FEM model of the aircraft, where the wingbox is modelled with a detailed GFEM while the other components are modelled as stick elements. This model was used to perform linear gust analyses in Nastran with the hinge locked and released. The results of this HI-FI structural solution are used to compare the wing failure indexes in the two conditions, assessing the effectiveness of the GLA.

1 INTRODUCTION

In the latest years, the research on high aspect ratio wings [1]-[10] stimulated the aeroelastic community producing a lot of work on the design challenges the development of new tools to account for the increased flexibility and the experimental validation [11].If the benefits of increasing the Aspect Ratio are clear (reduced induced drag and improved aerodynamic efficiency), the drawbacks due to the slenderer wing are not negligible. The aerodynamic forces, particularly the bending moment, increase requiring more structural mass to withstands the loads; the increased flexibility may introduce aeroelastic instability that may jeopardize the aircraft (flutter, control reversal, divergence). In this framework, the U-HAWRWARD project [2][12] investigates different technologies to increase the aspect ratio of the aircraft, limiting the weight increase and accounting for the aeroelastic phenomena. In particular, two strategies for the gust load alleviation were investigated: an active Static Output Feedback (SOF) controller [13][14] that uses conventional control surfaces (ailerons and elevator) developed by Polimi, and a flared hinged folding wing tip (FWT) [15]-[18] investigated by the University of Bristol.

2 MODEL AND METHODS

This section describes the model used for the analyses, that are a stick FEM model coupled with a Doublet-Lattice (DLM) mesh through a set of Radial Basis Function (RBF) splines. In the case of the FWT, the hinge was introduced through an MPC mechanism to account for the free-floating wing tip, small elastic elements (CELAS) are placed on the hinges rotations degrees of freedom to decouple the FWT modes from the free-body dynamics of the aircraft. The resulting FWT rigid modes are illustrated in Figure 1. The analyses were performed with NeoCASS [19]-[21].

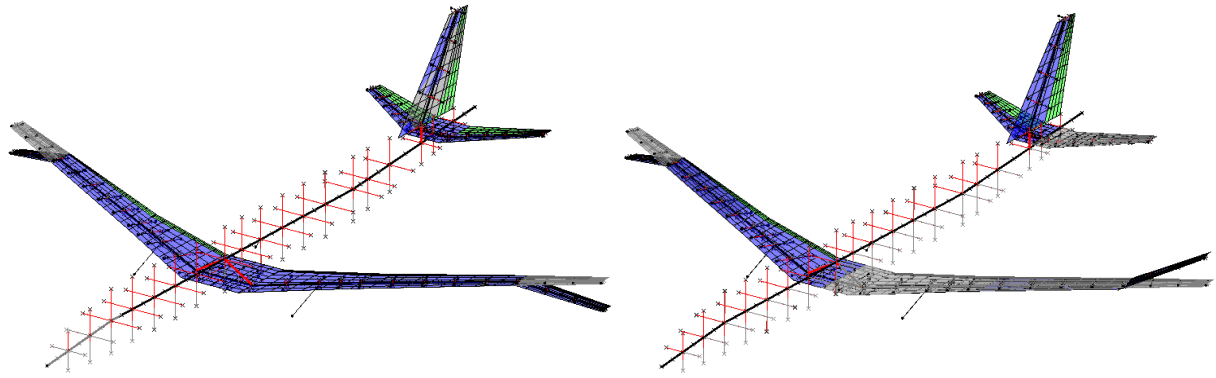

Figure 1: FWT modes at 0.04Hz: left symmetric and right anti-symmetric

To have a common base for the comparison between the two technologies, the FWT hinge spanwise position is in correspondence of the aileron, in this way the same wing span is used for the passive and active alleviation technologies. The aircraft aeroelastic model, with a detail of the hinge position and orientation is presented in Figure 2. The hinge orientation is the result of a parametric study [18] that optimizes its effectiveness.

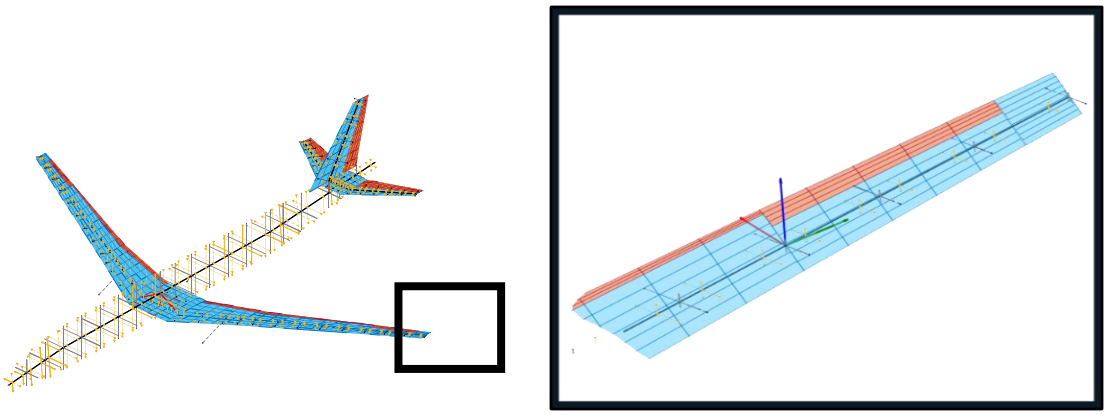

Figure 2: CNT AR15 stick model and the detail of the left wing with the coordinate system used to define the hinge.

The same model, with the hinge locked, was used to realize the baseline aircraft and the model equipped with the SOF controller. To implement the controller, the FEM model was translated into a SS-model thanks to the Matrix Fraction Approximation (MFA) [22] implemented in NeoCASS and used to identify the Generalized Aerodynamic Forces (GAFs) transfer function between the nodal forces and the structural motion, the external gust excitation, and the control surface deflection. The actuators were modelled with 2nd order low pass filters with 15Hz bandwidth and added to the aeroelastic system, leading to the aero-servo-elastic system of Eq. (1)

$$\begin{cases} \dot{\boldsymbol{x}} = \boldsymbol{A}\boldsymbol{x} + \boldsymbol{B}\boldsymbol{u} \\ \boldsymbol{y} = \boldsymbol{C}\boldsymbol{x} + \boldsymbol{D}\boldsymbol{u} \end{cases} \tag{1}$$

The controller is static because it directly uses the measured signals to generate the control input, except for a discrete integrator used to obtain the structural velocities. Its structure is the one in Eq.(2), where the ailerons are moved symmetrically and proportionally to wing tip and center of gravity accelerations and velocities, and the pitch rate. The elevator is moved proportionally to the pitch rate to alleviate the low frequencies gusts and to guarantee the stability of the rigid body modes.

$$\begin{Bmatrix} \delta_{aile\ RH} \\ \delta_{aile\ RH} \\ \delta_{elev} \end{Bmatrix} = -\begin{bmatrix} x_1 & x_2 & x_1 & x_2 & x_3 & x_4 & x_5 \\ x_1 & x_2 & x_1 & x_2 & x_3 & x_4 & x_5 \\ \square & \square & \square & \square & \square & \square & x_6 \end{bmatrix} \begin{Bmatrix} \ddot{x}_{tip\ RH} \\ \dot{x}_{tip\ RH} \\ \ddot{x}_{tip\ LH} \\ \dot{x}_{tip\ LH} \\ \ddot{x}_{CG} \\ \dot{x}_{CG} \\ q \end{Bmatrix} \Rightarrow \boldsymbol{u} = -\boldsymbol{G}\boldsymbol{y} \tag{2}$$

The procedure used to tune the SOF's gain matrix is the one presented in [23], a cost function *f* as in Eq.(3) is used. It is a weighted sum of the ratio between the open and closed loop (OL and CL respectively), bending and torsional moment (BM and TM) monitored on the wing root and engine section (WR and ES).

$$f = \frac{WRBM_{CL}}{WRBM_{OL}} + \frac{WRTM_{CL}}{WRTM_{OL}} + \frac{ESBM_{CL}}{ESBM_{OL}} + \frac{ESBM_{CL}}{ESBM_{OL}} \quad (3)$$

The constraints used during the optimization are the stability of the system, hence the closed loop state matrix eigenvalues and the ratio of the control surfaces, that saturate at $80\frac{^\circ}{s}$. Figure 3 shows the sensor and control surface layout used for the active GLA.

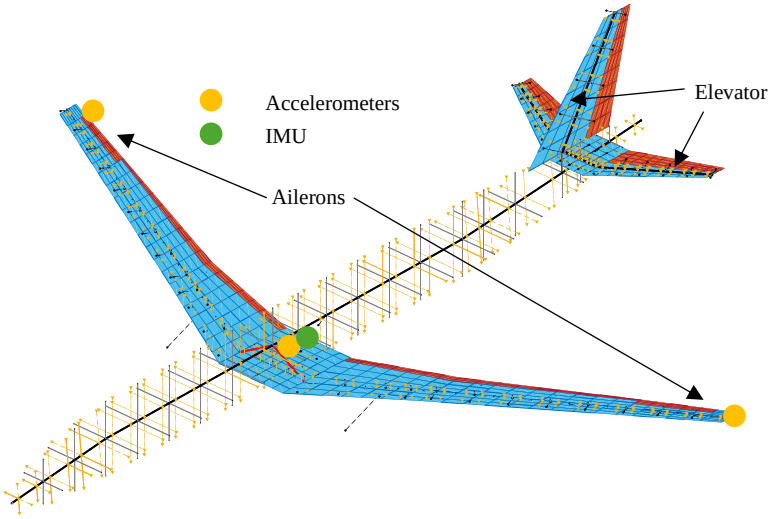

Figure 3: Sensor location and control surfaces used for GLA

3 NUMERICAL RESULTS

The models above described were analyzed to investigate the gust response. For each flight point and mass configuration, the 1-cosine gust input related to 10 equally spaced gust gradient between 9m and 107m where studied, for both positive and negative gust amplitude. The gust shape is obtained as prescribed by EASA/CS25 regulation [24], for sake of simplicity and to be conservative, the flight profile alleviation factor, Fg, was considered equal to 1. The gust shape, for different flight points and gust gradients can be obtained ai in Eqs.(4)(5)

$$U_{ds} = \sqrt{\frac{\rho_z}{\rho_0}} F_g U_{REF} \left(\frac{H}{107}\right)^{\frac{1}{6}} \quad (4)$$

$$U_{gust} = \frac{U_{ds}}{2}\left(1 - \cos\left(\frac{\pi V_\infty}{H} t\right)\right) \quad (5)$$

The six flight points considered are equivalent to a cruise speed of EAS=150m/s for altitudes going from 0m to 10000m with a step of 2000m. The four mass configurations considered are reported in Table 1. For each gust, four time-correlated loads are obtained: maximum and minimum bending and torsional moments. This led to an envelope of 4 mass configurations, 6 flight points, 20 gusts, 4 loads for each gust that results in 1920 load conditions.

Table 1: mass configuration considered for the gust analysis

Mass Configuration	Payload	Fuel
CONF1	100%	80%
CONF2	80%	100%
CONF4	100%	0%
CONF5	50%	100%

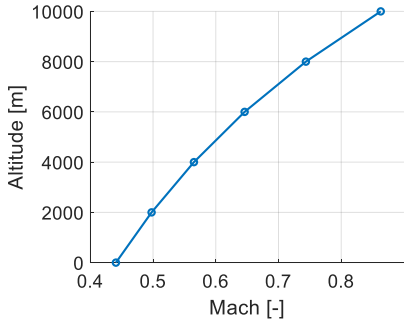

Figure 4: Flight Points considered for gust analysis

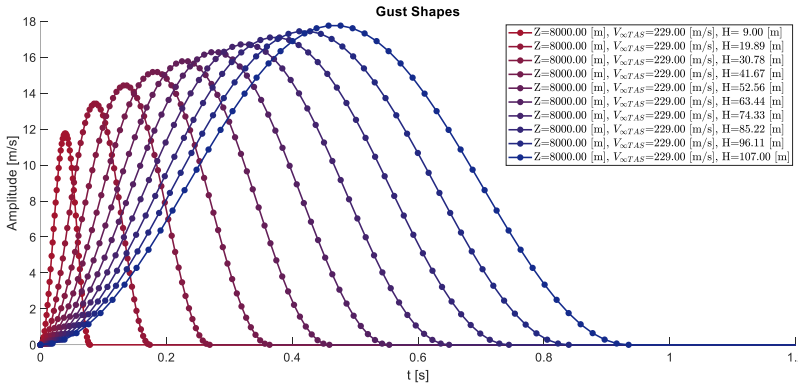

Figure 5: Gust shapes at z=8000m and TAS=229m/s

To compare the load alleviation capabilities, the wing root bending and torsional moment were enveloped for the cantilevered (CNT), folding wingtip (FWT) and cantilevered with gust load alleviation (GLA) configurations. The flight and mass envelopes considered are presented in Table 1 and Figure 4.

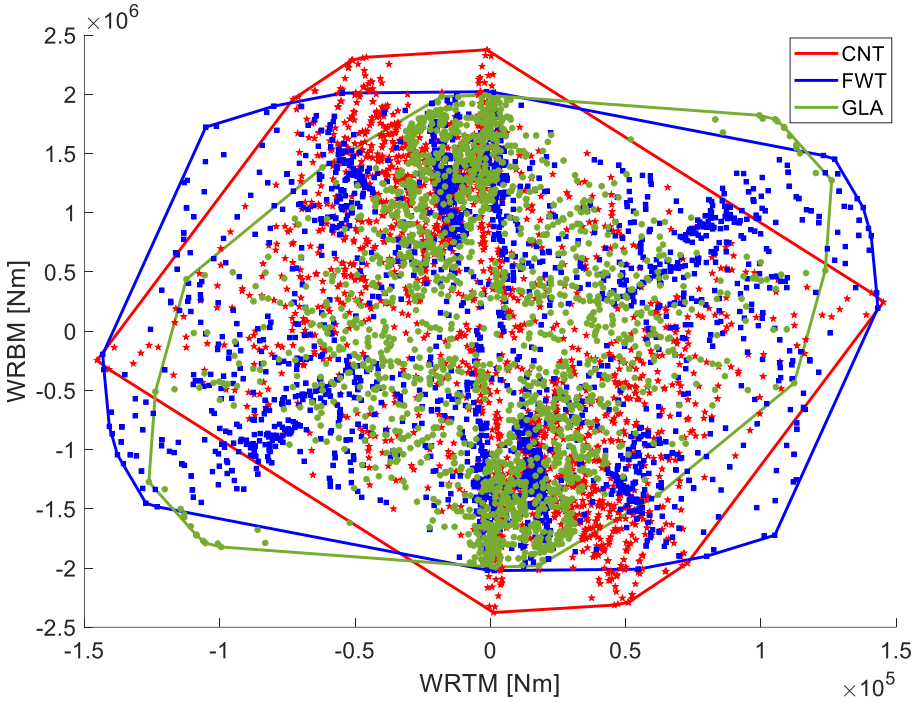

Figure 6: Torsional-Bending moment envelope at the wing root

Table 2: Alleviation comparison at the wing root

Configuration	WRBM	WRTM
CNT	-	-
FWT	-14.9%	-1.4%
GLA	-16.1%	-13.2%

Both FWT and GLA can reduce the WRBM up to a 15%, with slightly better performances for the GLA, which alleviate also the WRTM while the FWT impact on this component is negligible.

Despite the overall WRBM envelope reduction for the FWT is around 15%, a drawback of this technology arises. While comparing the time responses of the WRBM, is it possible to see that the peak value is reduced but the damping of the response is lower, as Figure 7 shows. From one side, the FWT helps in reducing the sizing loads, but it increases the fatigue in the components.

An explanation of this is shown in Figure 8, that represents a comparison of the transfer function between the gust input and the WRBM for a cruise condition. It is clear that the mode at 2Hz, related to the first wing bending, is less damped when the hinge is released. Physically, it is missing the damping action of the outer wing.

The phenomenon is more evident for a gust gradient of 58m, equivalent to a gust frequency of 1.97Hz, close to the resonance peak in the transfer function.

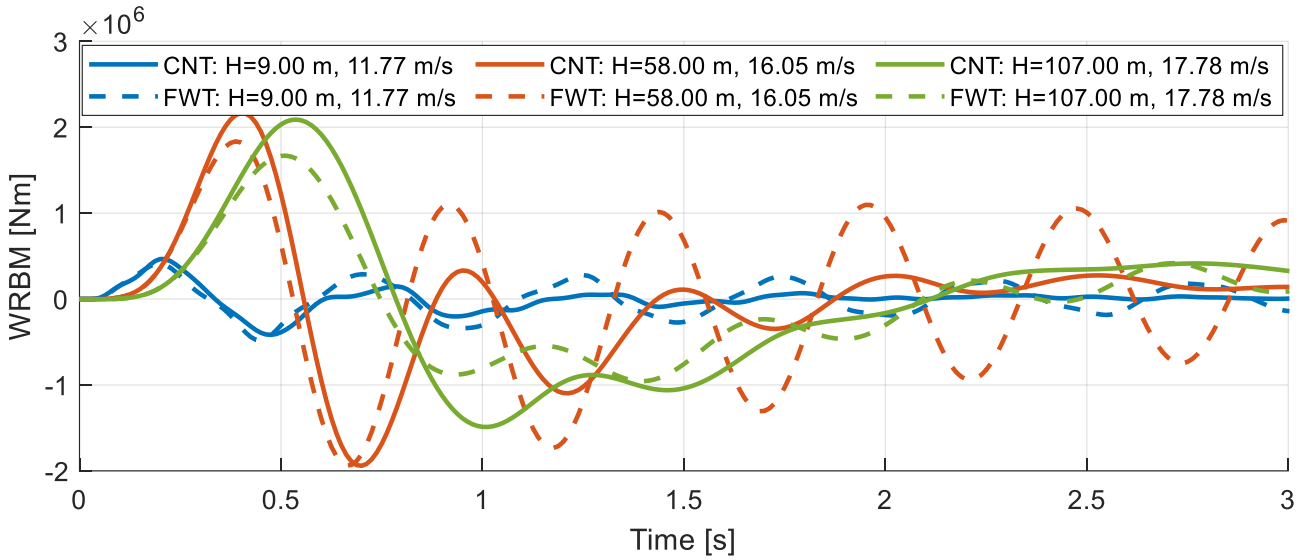

Figure 7: Time response for three gust gradients at z=8000m, VTAS=229m/s

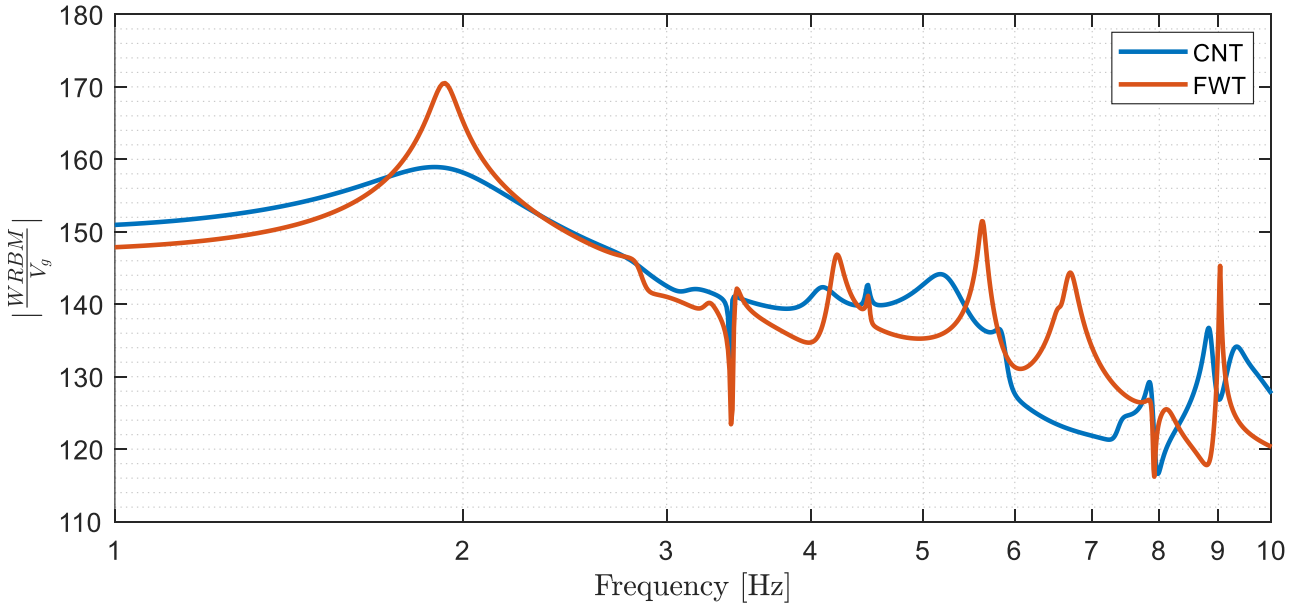

Figure 8: Transfer Function between the gust angle and the WRBM, z=8000m and VTAS=229m/s.

To assess the stability of the system, a flutter analysis of CNT and FWT was performed, producing the V-g plots of Figure 9: the damping reduction identified by the WRBM analyses is clear here, the 1st bending mode of the FWT has a reduction of the aeroelastic damping between 160 and 220 m/s. Despite the stability is guaranteed, the damping evolution of the FWT over the flight envelope identifies a zone where the system struggles to reduce the vibration, introducing fatigue possible fatigue problems. The cruise condition considered is at 229m/s that is close to this area, and combined to the quasi-tuned gust with H=58m, results in a low damped WRBM as shown in Figure 7.

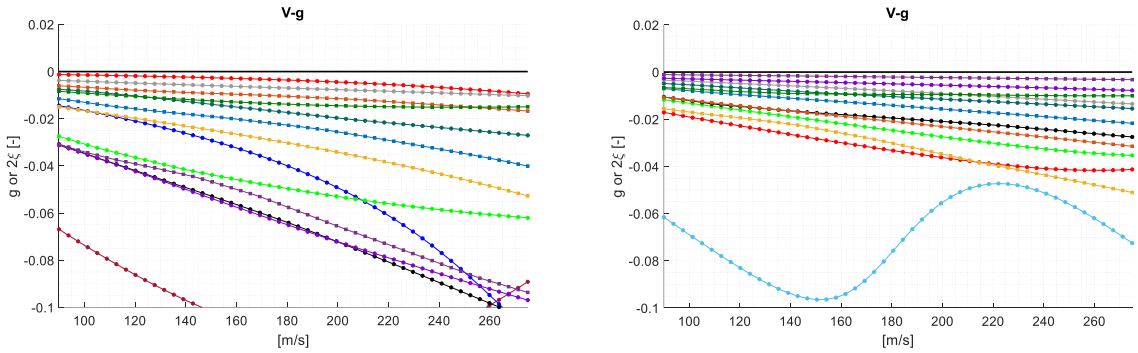

Figure 9: V-g plot for CNT (left) and FWT (right), z=8000m

4 HIGH FIDELITY MODEL

NeOPT produces a detailed Nastran FEM model of the wingbox [5], which was substituted to the wing's stick model in the aircraft model, creating a hybrid model. This kind of model has stick elements for the fuselage and the tail planes, while the wingbox is entirely modelled with its high-fidelity FEM model. The skins, ribs and spar webs are modelled with composite (PCOMP) plates (CQUAD4) with the stacking sequence of Figure 10, while the stringer and spar caps are modelled with bar elements (CBAR). The non-structural mass distribution (fuel and payload) is represented with concentrated masses (CONM2). Since the model is analysed with Nastran, the aerodynamic method used is the Doubled Lattice Method (DLM). The model was realized both for the CNT wing and for the wing equipped with the FWT. The resulting hybrid model is shown in Figure 11, while Figure 12 illustrates the components of the detailed wingbox FEM. Figure 13 shows the hinge mechanism for the IWT that is realized through MPC as in the stick model. The rigid modes of the two FWT are shown in Figure 14.

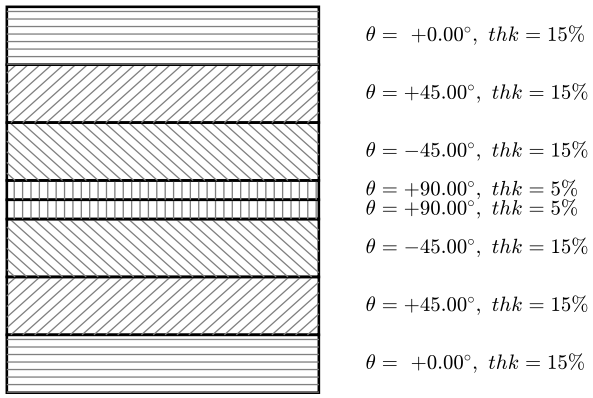

Figure 10: Stacking sequence for the composite components

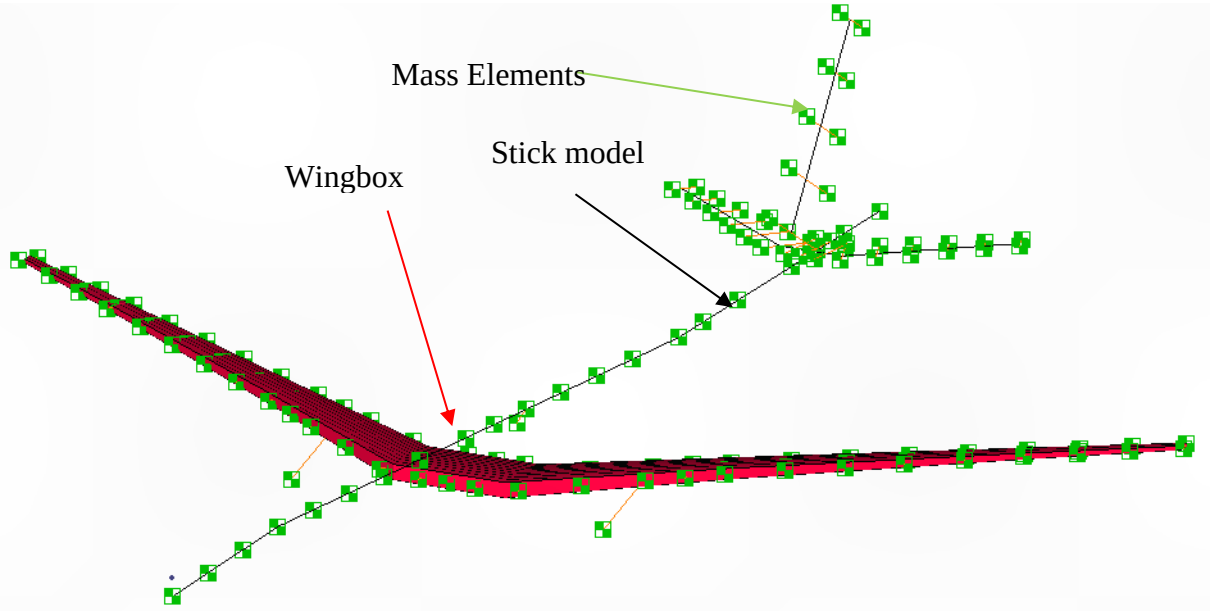

Figure 11: Hybrid Model

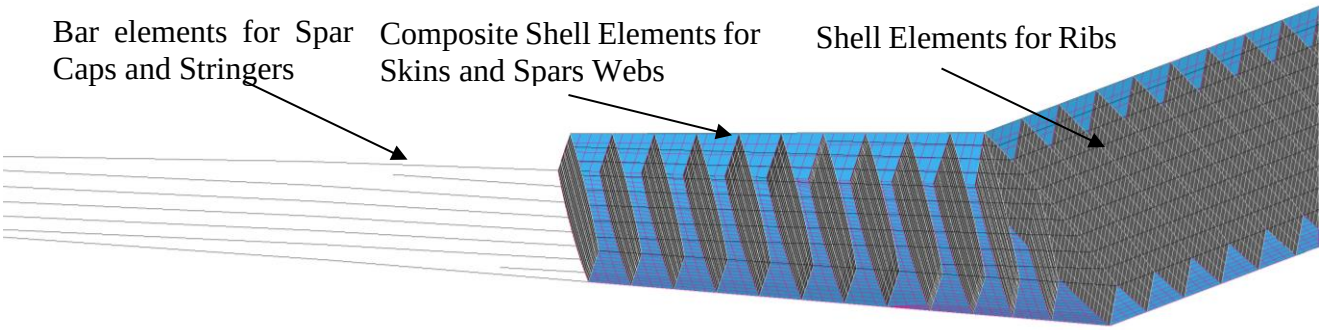

Figure 12: Detail of the Wingbox GFEM

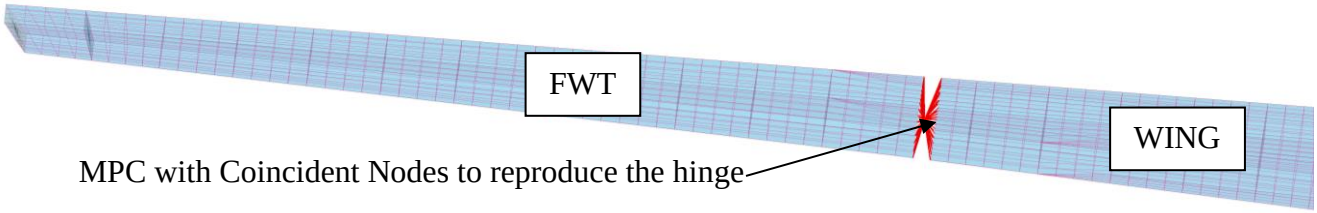

Figure 13: Modeling of the FWT hinge

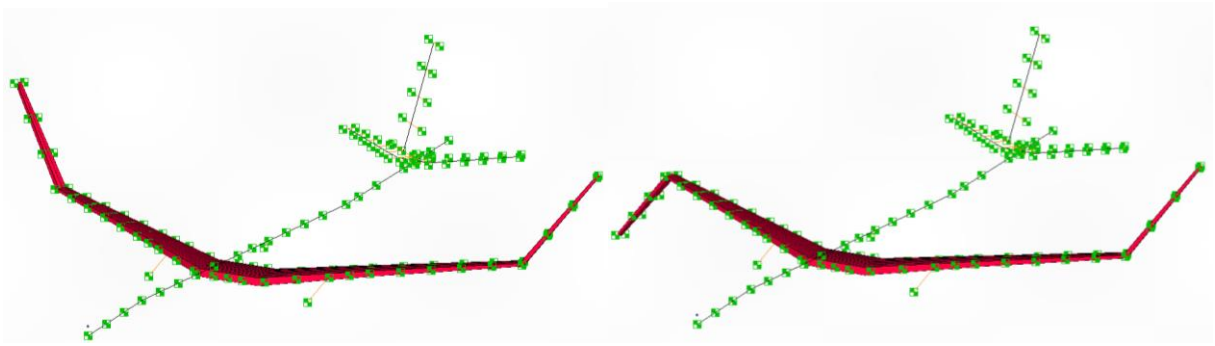

Figure 14: FWT modes for the Hybrid Model, both at 0.04Hz

Computational effort for this model is way more expensive with respect to the stick model, for this reason the gust analysis is performed for a single flight point, considering three different gust length (H=9, 58, 107m). The flight point is the cruise at 8000m, with a TAS of 229.09 m/s and a Mach number of 0.74.

To compare the behavior of the GFEM with respect to the stick model, the time responses of the displacement for three different spanwise section were compared. The first section is the wing root, the second is the FWT hinge while the last one is the wing tip.

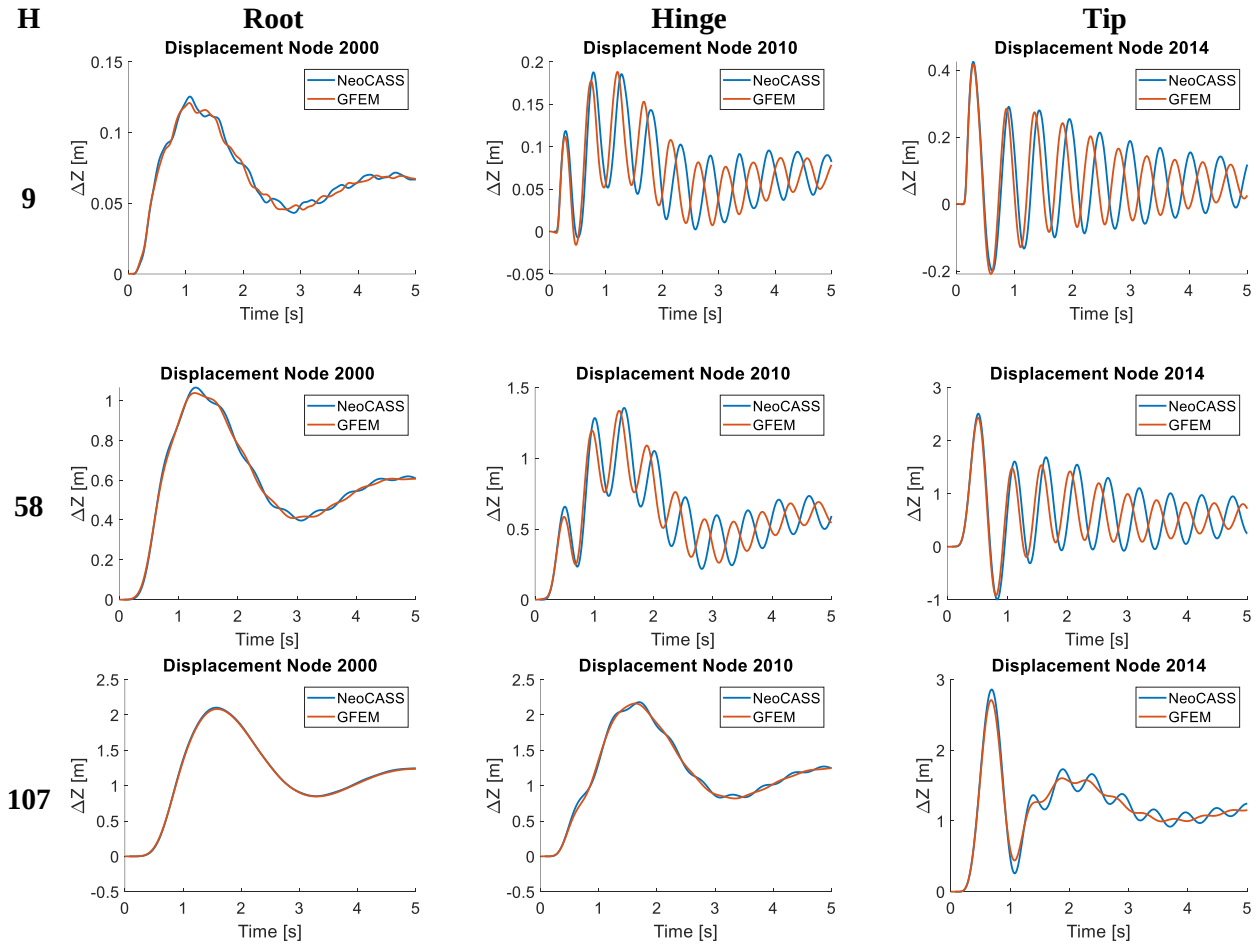

Figure 15: Comparison of the displacement obtained for the Hybrid and Stick models

The responses in term of vertical displacement are quite similar for the peak value, a shift in frequency is evident and it can be related to a difference in the first wing bending mode, which appear to be stiffer, and the mass distribution is slightly different. In fact, the 1st bending of the GFEM is at 2.034Hz, while it is at 1.896Hz for the stick model. In general, the responses are quite similar, meaning that the GFEM and the stick model are correlated.

4.1 Failure Index analysis

For the GFEM it is possible recover stress and strain information rather than the time evolution of the internal forces. The Failure Index (FI) is an indicator of how much dangerous a load condition is, in this case it is used to evaluate the difference between the solution obtained for the CNT and FWT configurations. The failure index is monitored on an element of the upper skin close to the wing root, but sufficiently far from the carrythrough so that boundary effects vanish (Figure 16). The gust and the flight point considered are the one used to compare the stick model and hybrid model displacement in the previous section.

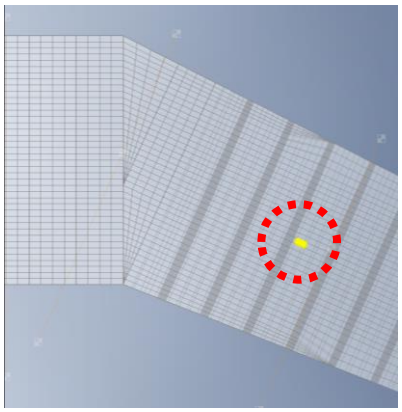

Figure 16: element considered to monitor the FI

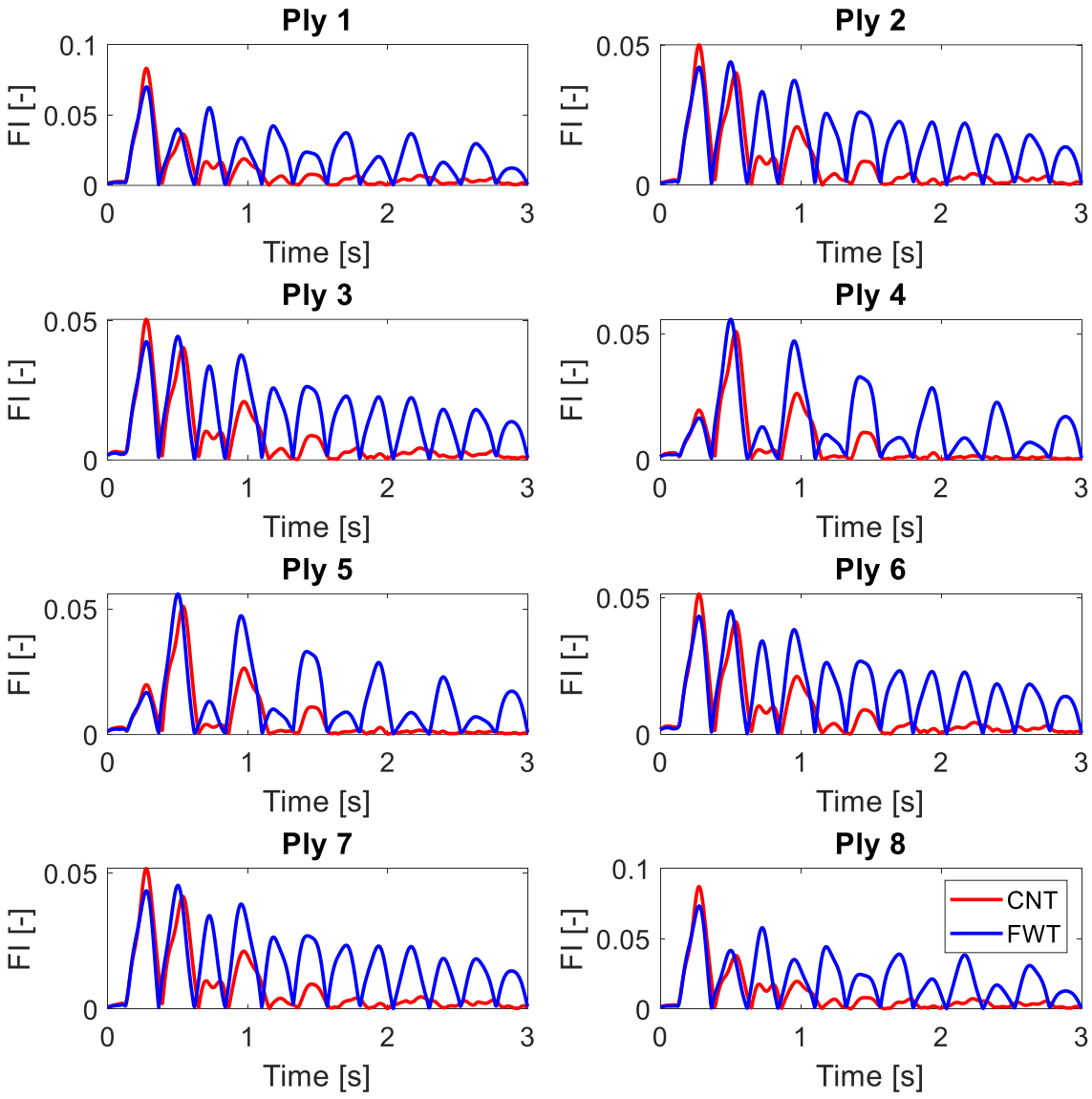

Figure 17: FI comparison, H=58m, Z=8000m, VTAS=229m/s

From Figure 17 is it possible to see how the most critical failure indexes, i.e. the ones of plies 1 and 8 are lowered by the FWT, but the oscillatory behaviour highlighted in Section 4 is present also for the FI. This may introduce criticalities from the fatigue point of view and must be taken into consideration in the design. Possible mitigation action of such phenomena will be discussed in the conclusions.

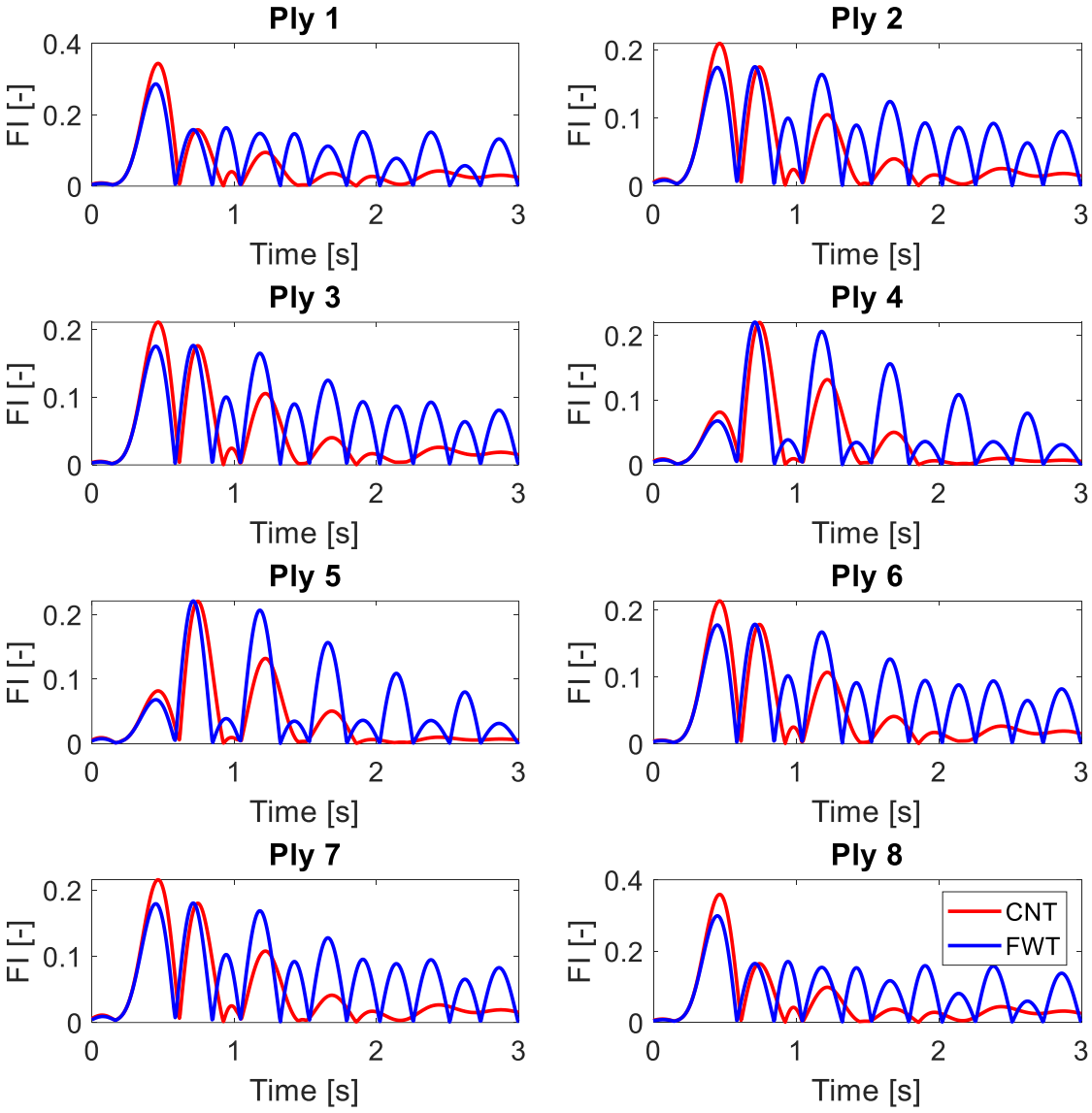

Figure 18: FI comparison, H=58m, Z=8000m, VTAS=229m/s

From Figure 18, but also from Figure 17 and Figure 22, it is possible to see that the more critical ply for the stacking sequence is the Ply#1, which is the one with the fiber oriented at 0° (parallel to the wingspan). The following figures (Figure 19 and Figure 20) compares the axial stress distribution for Ply#1 at the instant where the FI is higher (t=0.45s from Figure 18) for both the CNT (left wing) and FWT (right wing) configurations. The scale used for the stress is the same for a direct comparison between the two solutions. Figure 21 compares the deformed shape of the two configurations at the peak's value instant.

Is it clear that the overall stress distribution on the wing is lower for the FWT when the gust peak occurs, and it is a direct consequence of a lower internal force acting on the wing as shown by Figure 7 for the stick model.

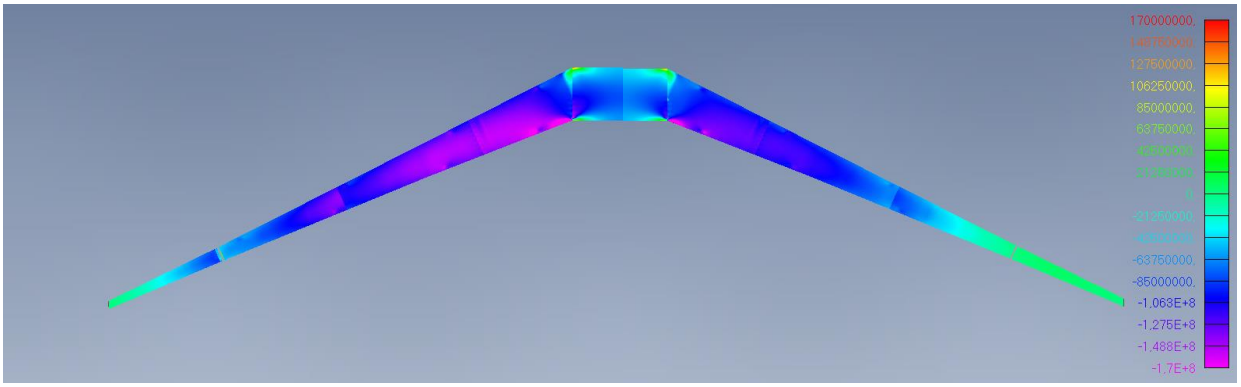

Figure 19:CNT (LH) vs FTW (RH), H=58m, Z=8000m, VTAS=229m/s, t=0.45s, $\sigma_{ply1,x}$ skin upper

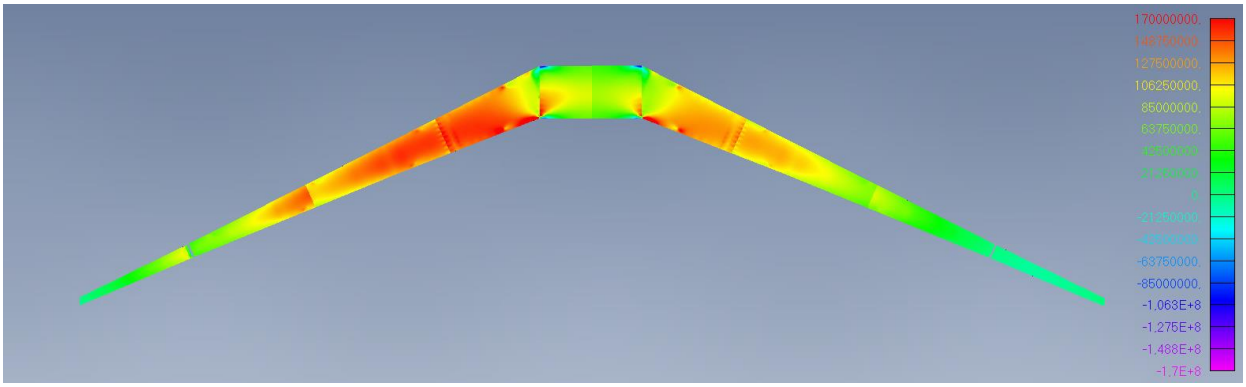

Figure 20: CNT (LH) vs FWT (RH), H=58m, Z=8000m, VTAS=229m/s, t=0.45s, $\sigma_{ply1,x}$ skin lower

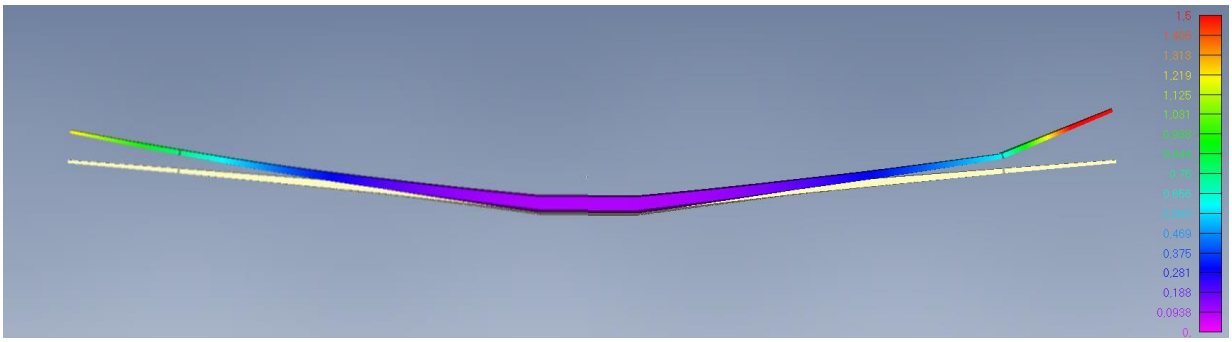

Figure 21: CNT (LH) vs FWT (RH), H=58m, Z=8000m, VTAS=229m/s, t=0.45s, deformed shape

In the case of a lower frequency gust (Figure 22), with gust gradient H=107m equivalent to 1.07Hz, the FI are lower and damped for the FWT. In fact, the gust excitation is separated from the 1st wing bending mode (around 2Hz), as it is possible to see from Figure 8.

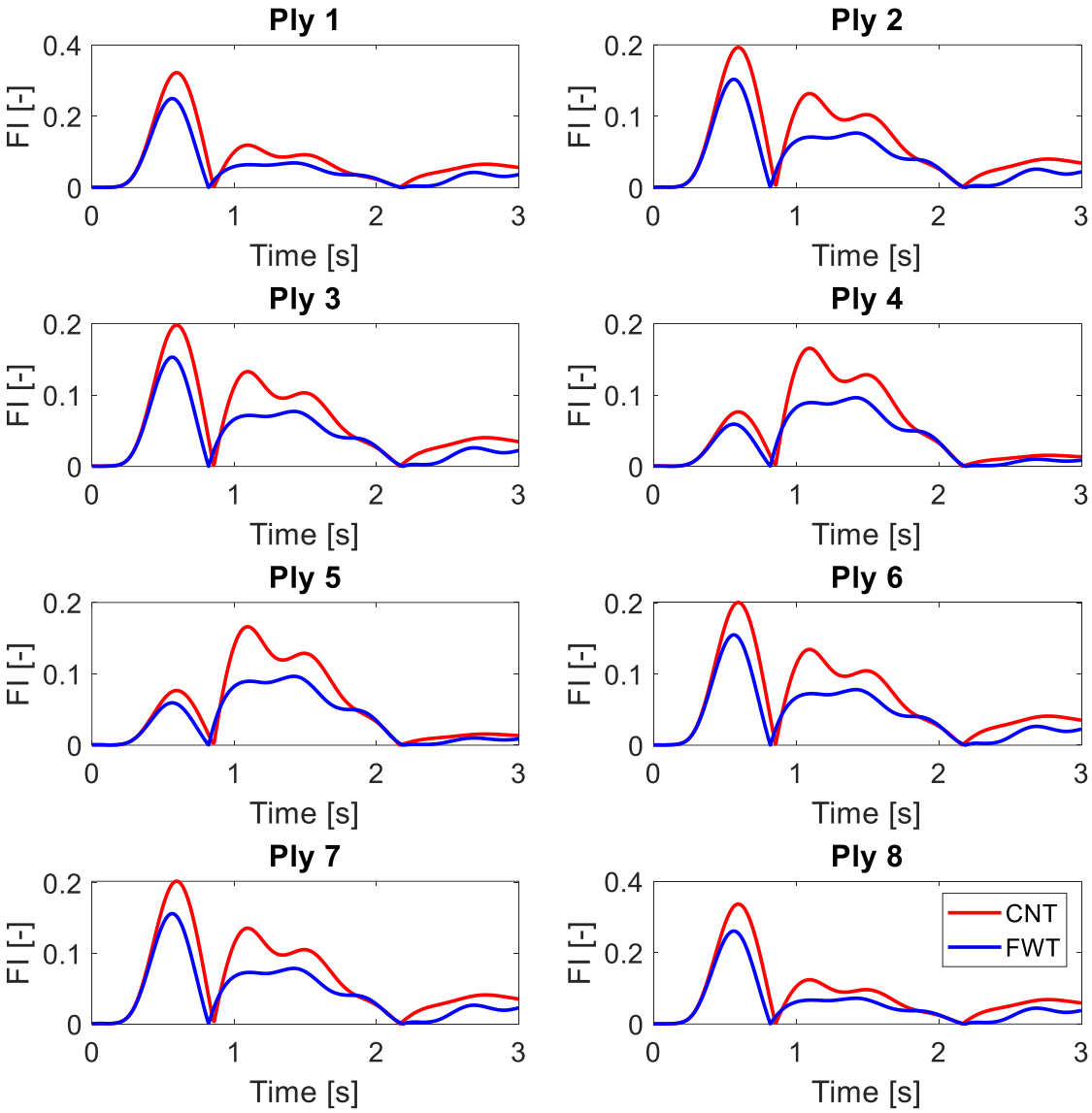

Figure 22: FI comparison, H=107m, Z=8000m, VTAS=229m/s

5 CONCLUSIONS

This paper compared the effect of active (GLA) and passive (FWT) gust load alleviation technologies. The first part of the work showed how a reduction of 15% in WRBM gust envelope can be obtained with the alleviation for both the cases, with a reduction of the WRTM more efficient for the GLA (13%) with respect to the FWT (1.4%).

The FWT showed a less damped aeroelastic 1st bending mode, and this reflects into a less damped time response of the excited wing over a certain and frequency range. This depends also on the flight speeds, as shown in the flutter analysis. Despite the peak value in term of loads is lower, persistent oscillations are present. This is critical for the fatigue and a tradeoff between the load reduction and the fatigue life must be done to fully assess the benefit of the FWT concept. This aspect will be further investigated considering different hinges mechanisms, for example equipped with dampers, to improve the damping of the free floating FWT.

Finally, the detailed wingbox FEM integrated into the stick model provided information about the failure indexes and the stresses in the wing, showing that the FWT has lower FI concerning the gust response and there is room for improving the structural solution by using such technology, similarly to what can be achieved with the active load control.
FWT is more recent than GLA and many aspects of this technology need to be investigated, for example this paper shows that the fatigue of a wing with FWT cannot be neglected since it may become a relevant sizing factor for the wing design.

REFERENCES

[1] Carrier, G. G., Arnoult, G., Fabbiane, N., Schotte, J. S., David, C., Defoort, S., ... & Delavenne, M. (2022). Multidisciplinary analysis and design of strut-braced wing concept for medium range aircraft. In AIAA SCITECH 2022 Forum (p. 0726).

[2] Ricci, S., Paletta, N., Defoort, S., Benard, E., Cooper, J. E., & Barabinot, P. (2022). U-HARWARD: a CS2 EU funded project aiming at the Design of Ultra High Aspect Ratio Wings Aircraft. In AIAA Scitech 2022 Forum (p. 0168).

[3] Ricci, S., Marchetti, L., Toffol, F., Beretta, J., & Paletta, N. (2022). Aeroelastic Optimization of High Aspect Ratio Wings for Environmentally Friendly Aircraft. In AIAA Scitech 2022 Forum (p. 0166).

[4] Toffol, F., & Ricci, S. (2023). Preliminary Aero-Elastic Optimization of a Twin-Aisle Long-Haul Aircraft with Increased Aspect Ratio. Aerospace, 10(4), 374.

[5] Toffol, F., & Ricci, S. (2023). A Meta-Model for composite wingbox sizing in aircraft conceptual design. Composite Structures, 306, 116557.

[6] Martins, J. R., Kennedy, G., & Kenway, G. K. (2014). High aspect ratio wing design: Optimal aerostructural tradeoffs for the next generation of materials. In 52nd Aerospace Sciences Meeting (p. 0596).

[7] Tang, D., & Dowell, E. H. (2002). Experimental and theoretical study of gust response for high-aspect-ratio wing. AIAA journal, 40(3), 419-429.

[8] Sanghi, D., Cesnik, C. E., & Riso, C. (2024). Roll Maneuverability of Transonic High-Aspect-Ratio-Wing Aircraft with Flared Folding Wingtips. Journal of Aircraft, 1-14.

[9] Afonso, F., Vale, J., Oliveira, É., Lau, F., & Suleman, A. (2017). A review on non-linear aeroelasticity of high aspect-ratio wings. Progress in Aerospace Sciences, 89, 40-57.

[10] Abouhamzeh, M., Ma, Y., & Elham, A. (2022). A Geometrically Nonlinear Structural Model For Aerostructural Optimization of Ultra-High Aspect Ratio Composite Wings. In AIAA SciTech 2022 Forum (p. 0724).

[11] Marchetti L., Ricci S., Riccobene L., Grassi D., Mantegazza P., Adden S., Gu H. and Cooper J. Gust load alleviation wind tunnel tests of a folding wing tip configuration, International Forum of Aeroelasticity and Structural Dynamic, The Hague, 17-20 June 2024.

[12] Cooper, J. E., Gu, H., Ricci, S., Toffol, F., Adden, S., Meheut, M., ... & Barabinot, P. (2024). CS2-THT U-HARWARD Project: Final Assessment and Project Outcomes Evaluation. In AIAA Scitech 2024 Forum (p. 2111).

[13] Fonte, F., Ricci, S., & Mantegazza, P. (2015). Gust load alleviation for a regional aircraft through a static output feedback. Journal of Aircraft, 52(5), 1559-1574.

[14] Toffol, F., Marchetti, L., Ricci, S., Fonte, F., Capello, E., & Malisani, S. (2023). Gust and Manouvre Loads Alleviation Technologies: Overview, Results and Lesson Learned in the Framework of the Cs2 Airgreen2 Project. In 19th International Forum on Aeroelasticity and Structural Dynamics (IFASD 2022) (pp. 1-24).

[15] Castrichini, A., Cooper, J. E., Wilson, T., Carrella, A., & Lemmens, Y. (2017). Nonlinear negative stiffness wingtip spring device for gust loads alleviation. Journal of Aircraft, 54(2), 627-641.
[16] Healy, F., Gu, H., Rezgui, D., & Cooper, J. E. (2024). Nonlinear Stability Analysis of Floating Wingtips with Control Surface Freeplay. In AIAA SCITECH 2024 Forum (p. 1267).
[17] Gu, H., Healy, F., Jayatilake, S., Rezgui, D., Lowenberg, M., Cooper, J., ... & Castrichini, A. (2024). Flight Dynamics of Aircraft Incorporating the Semi-Aeroelastic Hinge. Aerospace Science and Technology, 109026.
[18] Gu, H., Healy, F., Rezgui, D., & Cooper, J. (2023). Sizing of high-aspect-ratio wings with folding wingtips. Journal of Aircraft, 60(2), 461-475.
[19] Cavagna, L., Ricci, S., & Travaglini, L. (2011). NeoCASS: an integrated tool for structural sizing, aeroelastic analysis and MDO at conceptual design level. Progress in Aerospace Sciences, 47(8), 621-635.
[20] Cavagna, L., Ricci, S., & Travaglini, L. (2011). Aeroelastic analysis and optimization at conceptual design level using NeoCASS suite. In 52nd AIAA/ASME/ASCE/AHS/ASC Structures, Structural Dynamics and Materials Conference 19th AIAA/ASME/AHS Adaptive Structures Conference 13t (p. 2079).
[21] Fonte, F., & Ricci, S. (2019). Recent developments of NeoCASS the open source suite for structural sizing and aeroelastic analysis. In 18th International Forum on Aeroelasticity and Structural Dynamics (IFASD 2019) (pp. 1-22). International Forum on Aeroelasticity and Structural Dynamics (IFASD).
[22] Ripepi, M., & Mantegazza, P. (2013). Improved matrix fraction approximation of aerodynamic transfer matrices. AIAA journal, 51(5), 1156-1173.
[23] Ricci, S., Toffol, F., De Gaspari, A., Marchetti, L., Fonte, F., Riccobene, L., ... & Morgansen, K. (2022). Wind tunnel system for active flutter suppression research: Overview and insights. AIAA Journal, 60(12), 6692-6714.
[24] EASA, Certification Specification for Large Aeroplanes CS-25

AKNOWLEDGEMENTS

The U-HARWARD Project has received funding from the Clean Sky 2 Joint Undertaking, under the European's Union Horizon 2020 research and innovation Program under Grant Agreement number: 886552 - H2020 -CS2-CFP10-2019-01.
The support of J. E. Cooper and H. Gu from University of Bristol is highly appreciated.

COPYRIGHT STATEMENT